GA 1485 (REV. 10/82) ROLL 1457 A

GA Technologies Inc.

ISSUE SUMMARY

TITLE METALLOGRAPHIC EXAMINATION OF A FUEL ROD FROM SEGMENT 2 FSV FUEL ELEMENT 1-2415

☐ R & D
☒ DV & S
☐ DESIGN

APPROVAL LEVEL 2

DISCIPLINE	SYSTEM	DOC. TYPE	PROJECT	DOCUMENT NO.	ISSUE NO./LTR.
N	18	RTE	1900	906968	A

QUALITY ASSURANCE LEVEL	SAFETY CLASSIFICATION	SEISMIC CATEGORY	ELECTRICAL CLASSIFICATION
QAL-I	SC-2	CAT-I	N/A

1 RELEASED

ISSUE	DATE	PREPARED BY	APPROVAL				ISSUE DESCRIPTION/ CWBS NO.
			ENGINEERING	QA	FUNDING PROJECT	APPLICABLE PROJECT	
A	NOV 0 9 1983	F. McCord 11/8/83	W.J. Scheffel 11-8-83 Scheffel; O.M. Stansfield 11-8-83 Stansfield; D. Alberstein 11/8/83 D.Alberstein	G.P. Connors 11/8/83	D.J.Kowal 11-8-83	D.J.Kowal 11-8-83	Initial issue from originating project No. 2970 100 004

CONTINUE ON GA FORM 1485-1

NEXT INDENTURED DOCUMENTS

P.O.N-4567

REV																											
SH																											
REV																											
SH	29	30	31	32	33	34	35	36	37	38	39	40	41	42	43	44	45	46	47	48	49	50	51	52	53	54	55	56
REV																											
SH	1	2	3	4	5	6	7	8	9	10	11	12	13	14	15	16	17	18	19	20	21	22	23	24	25	26	27	28

Notations in this column indicate where changes have been made

TITLE: METALLOGRAPHIC EXAMINATION OF A FUEL ROD FROM SEGMENT 2 FSV FUEL ELEMENT 1-2415

Document No. 906968 | Issue A

TABLE OF CONTENTS

LIST OF TABLES

LIST OF FIGURES

TITLE: METALLOGRAPHIC EXAMINATION OF A FUEL ROD FROM SEGMENT 2 FSV FUEL ELEMENT 1-2415

Document No. 906968 | Issue A

1. INTRODUCTION

During the core segment 2 surveillance in April of 1982 at the Fort St. Vrain (FSV) reactor site, fifty-four fuel and reflector elements were metrologically and visually inspected. The metrological inspections were carried out using the metrology robot described in Reference 1. The visual inspections employed four remotely controlled television cameras equipped with pan-tilt units and zoom lenses. All element surfaces were thoroughly inspected, and recorded on videotape and on 35 mm photographic film. A hairline axial crack was observed extending the entire block length in the center of face B (see Figure 1) of the element S/N: 1-2415 (core location 08.05.F.06). Later inspection of the videotapes and photographs revealed a second element S/N: 1-0172 with a suspected similar crack in face B, later confirmed by examination in the GA Hot Cell (Ref. 2). This block was located one layer lower, directly beneath element S/N: 1-2415 at core location 08.05.F.07.

To characterize better the cracks and determine why they occurred, the two blocks with cracked webs, along with three other blocks of potential interest, were shipped to the GA Technologies, Inc. hot cell for visual and destructive examinations. The visual examinations were completed and reported in Reference 2. Element S/N: 1-2415 was selected for postirradiation destructive examination as part of the US DOE - funded HTGR Technology Program (Ref. 3). This block was selected because it exhibited the wider crack, and it experienced larger fast fluence and metrological changes (see Table 1). Fuel rod metallography, which was not part of the DOE program, was funded by Public Service of Colorado to meet its commitments to NRC regarding fuel surveillance (Ref. 4). This report covers the fuel metallography portion of the postirradation destructive examination.

2. BLOCK (S/N: 1-2415) BACKGROUND

2.1 Element Description

Element S/N: 1-2415 consisted of a standard H-327 graphite fuel body having 210 fuel holes, 6 burnable poison holes, and 108 coolant channels (see

Figure 2). There was no lumped burnable poison installed in the element. The element contained 3132 fuel rods consisting of (Th,U)C_2 TRISO[a] fissile particles and ThC_2 TRISO fertile particles bonded together in a carbonaceous matrix. These TRISO coated particles were formed into fuel rods from fuel rod batch CR16N-10167, blend 1. The nominal preirradiation dimensions of the fuel rods were 12.5 mm (0.49 in.) in diameter and 49.3 mm (1.94 in.) in length. Fuel rod and fissile and fertile particle nominal attributes are given in Tables 2, 3, and 4, respectively.

2.2 Element History

The element was irradiated in region 8, column 5, core layer 6 (third layer from top of the active core). Figure 3 shows this core location (08.05. F.06). This element was part of the initial core (segment 2). Prior to February 1, 1979, when the reactor was shutdown for the first refueling, the initial core had operated for 174 effective full-power days (EFPD). Cycle 2 operation began on May 26, 1979 and was completed on May 13, 1981 after having accumulated a total of 189 EFPD. Thus, when element S/N: 1-2415 was removed from the core, it had accumulated a total of 363 EFPD. The average fast fluence[b] accumulated by the element was approximately 1.55×10^{25} n/m^2 (E > 29 fJ)$_{HTGR}$ with a peak of about 1.79×10^{25} n/m^2. The calculated time and volume-averaged graphite temperature was 650°C, with a peak graphite temperature of 700°C[c]. The calculated time average fuel temperature was 765°C.[c]

(a) In the TRISO particle design, a layer of SiC is sandwiched between two layers of high-density pyrolytic carbon, which provides a composite pressure vessel to retain gaseous fission products. The SiC coating also provides a barrier against the diffusion of metallic fission products and increases the mechanical and dimensional stability of the particle during irradiation. An inner low-density, or buffer, coating adjacent to the fuel kernel provides a void volume to accommodate fission gases and kernel swelling and, in addition, attenuates fission product recoils.

(b) Fast neutron fluence was obtained from the GATT code fuel accountability analyses for cycles 1 and 2. The fast neutron fuence was volume averaged (Ref. 1).

(c) These temperatures were obtained from SURVEY code calculations which use input from GAUGE code depletion analyses (Ref. 1).

TITLE: METALLOGRAPHIC EXAMINATION OF A FUEL ROD FROM SEGMENT 2 FSV FUEL ELEMENT 1-2415

3. METALLOGRAPHY

The metallographic examination was performed in accordance with the procedure outlined in Reference 5. Irradiated fuel rod 13 from fuel stack 308 was subjected to metallographic examination because it was expected to have a high temperature history relative to the fuel elsewhere in the element and, thus, would provide an indication of thermal effects in the fuel earlier than fuel rods from lower temperature portions of the element. This fuel rod, which was one rod length above the bottom of the fuel hole, came from the axial location in the block where the power peaked (Ref. 6). Fuel stack 308 was chosen because it was located under the dowel pin of face B adjacent to the cracked web. Figure 4 shows the location of fuel stack 308 in reference to the cracked web. In general, the appearance of the fuel rods from stack 308 was good, with no evidence of fuel rod-block interaction. A little chipping at the ends of the rods and some debonding of particles from the rod were observed (see Fig. 5). Rods which were chipped and slightly debonded on the ends appeared similar to the preirradiated rods and are not believed to have been damaged during operation or by the extraction of the stack from the fuel block. This conclusion is further supported by the low pushout force ($\leq$7 lbs) required to remove the stack from the fuel element. Also, the small amount of debris collected from the emptied block is indicative of a lack of fuel rod-block interaction.

Rod 13 was mounted in resin, ground, and polished in the metallographic hot cell. Prior to examination, all polished sections were passivated with a 50/50 solution of HNO_3 and H_2O to decrease the rate of hydrolysis of the ThC_2 kernels. The entire polished surface of the rod was then examined.

4. METALLOGRAPHIC EXAMINATION RESULTS

The fuel rod matrix appeared to be in good condition. Minor cracking of the matrix end caps similar to the cracking observed in segment 1 and the acceptable preirradiated rods, was observed. The microstructure of the matrix

after irradiation is shown in Figure 6. The irradiated microstructure was similar to the microstructure observed for FSV fuel rods irradiated in the FSV fuel proof capsule F-30 (Ref. 7). The measured macroporosity for rod 13 was 17.5%. This value is within the (14-29%) range of macroporosities observed for fuel rods from capsule F-30 (Ref. 7). An example of a radial cross section showing the macroporosity in the matrix is shown in Figure 7.

The results of the metallographic examination of fuel rod 13 from fuel stack 308 are presented in Tables 5 and 6. The irradiation performance of the fissile and fertile TRISO coated particles was satisfactory as evidenced by the moderate coating failures and good thermal performance. The microstructures of typical particles after being exposed to a peak fast neutron fluence of approximately 1.79×10^{25} n/m^2 $(E > 29\ fJ)_{HTGR}$ and a time-averaged fuel temperature of 765°C, are shown in Figure 8. A total of 231 fissile and 184 fertile particles were examined.

Fuel dispersion was observed in 75% of the fissile and 5% of the fertile particles. An example of fuel dispersion is shown in Fig. 9. Fuel dispersion can be caused by chlorine which can diffuse through a permeable IPyC into the buffer during the SiC coating operation. Production records indicate that this fuel had relatively low density IPyC and a tendency to exhibit fuel dispersion.

The primary purpose of the metallography was to examine the fuel for thermal effects. In this regard the chemical behavior of the TRISO particle was acceptable. Kernel migration was not observed. Interaction of the SiC coating with fission products was observed in both particle types. Figure 10 shows examples of the SiC interaction. SiC interaction was observed in 3.9% of the $(Th,U)C_2$ particles and 3.3% of the ThC_2 particles. The reaction penetrated about 5 μm into the SiC layer for both particles types.

This kind of interaction is expected in carbide fuel, where rare earth fission products are released from the kernel and react with the SiC (Ref. 8).

However, the observed depth of reaction (~3 μm) was larger than the <1 μm expected depth based on the time-temperature history of the fuel. This rapid penetration rate may have been associated with fuel dispersion caused by chlorine trapped in the buffer layer during the SiC coating operation, as discussed above, and/or a higher operating temperature than the average calculated for the fuel element. Penetration depths on the order of 10 to 15 μm might lead to some volatile fission product metal release, but total coating failure and fission gas release would not increase (Ref. 8). The penetration depth measured for these particles is significantly less than these values. Since fuel dispersion in the fuel which will reside in the core for up to six cycles is much less than dispersion in these fuel particles, it is not expected that fission product-SiC interaction will have an impact on core performance. However, this phenomenon will be monitored in future FSV fuel surveillance so that any influence on core performance can be properly assessed.

In the course of metallography the mechanical condition of the coating can be observed, but conclusions from these data are difficult to draw because coating failure can be caused during manufacture and during the grinding and polishing procedure in connection with making a metallographic mount. There was evidence that some of the coating failures can be attributed to as-manufactured failures which occurred during coating or rod fabrication. This conclusion is supported by the appearance of failed particles. An example of this type of failed particle is shown in Figure 11 where the particle had the appearance of having been crushed and fuel rod matrix was pressed into the coating cracks at the time of manufacture. In this case as-manufactured failure rather than in-pile failure was indicated. However, unlike the metallographic results of Segment 1 (Ref. 9), there was partial coating failure which may have occurred in-pile as seen in Figure 12. Irradiation induced shrinkage of the pyrocarbon was apparently enhanced by the additional exposure of cycle 2 and both IPyC and OPyC failures were observed as expected from accelerated capsule results (Ref. 7). For purposes of comparing with prior work, counts of observed failed individual coatings are reported in Tables 5 and 6. These

values should be considered upper limits. The total coating failure with resulting gas release can be expected to be very low because circulating gas activity has remained consistently low and indicates virtually no particle failure. However, as noted in Tables 5 and 6, the actual number of total coating failures was not determined due to hydrolysis of the kernels in the fuel rod mount.

5. SUMMARY AND CONCLUSIONS

The performance of the fuel was acceptable. Specific observations and conclusions are summarized as follows:

1. Fuel rod 13 from stack 308 was in good condition although minor cracking in the matrix end caps and some debonding of particles from the rod surface were observed.

2. There was no fuel rod - block interaction as evidenced by the visual examination of the rods, by the small pushout force of the stack, and by the small amount of debris collected from the emptied block.

3. The measured macroporosity for rod 13 was 17.5%, which was within the (14-29%) range of macroporosites observed for fuel rods from capsule F-30.

4. A total of 231 fissile and 184 fertile particles from rod 13 were examined. For the $(Th,U)C_2$ and ThC_2 particles, respectively, the OPyC coating failure was 0.4% and 7.6%, and the SiC coating failure was 0.9% and 3.8%. However, these coating failures should be considered the upper limits since coating failures can be caused during manufacture and during the grinding and polishing procedure, as well as during irradiation.

5. The chemical behavior of the particles was acceptable. There was no kernel migration observed. However, there was evidence of fission product interaction with the SiC coating. 3.9% of the fissile particles and 3.2% of the fertile particles showed fission product - SiC interaction with a penetration depth of ~5 μm, which was higher than the expected value of <1 μm. The phenomena may have been caused by fuel dispersion resulting from chlorine trapped in the buffer layer during the SiC coating and/or by higher operating temperatures than the average calculated for the element.

6. Fuel dispersion, which is attributed to chlorine diffusing through a low density IPyC into the buffer layer during the SiC coating process, and IPyC debonding were observed in some of the TRISO $(Th,U)C_2$ and ThC_2 particles. Fuel dispersion and IPyC debonding did not detrimentally affect the performance of the particles.

6. REFERENCES

1. SAURWEIN, J. J., ''Nondestructive Examination of 54 Fuel and Reflector Elements from Fort St. Vrain Core Segment 2'', GA-A16829, October 1982, PSC transmittal to NRC P-83196, June 2, 1983.

2. KETTERER, J. W., ''Visual Examination Results of Segment 2 FSV Fuel Elements 1-2415, 1-0172, 2-2693, 1-0108 and 5-0801'', Document No. 906577, Issue B, April 4, 1983, PSC transmittal to NRC P-83196, June 2, 1983.

3. McCORD, F., ''Test procedure for the Destructive Examination of Fort St. Vrain Fuel Element 1-2415'', Document No. 906770, February 25, 1983.

4. LEE, O. R. (PSC) letter to John Collins (NRC), ''Commitment to FSV Fuel Surveillance'', P-83058, February 10, 1983.

5. SCHEFFEL, W. J., ''Hot Cell Metallographic Examination of Irradiated Fuel Rods'', Document No. 904199, Issue A, October 8, 1979.

6. ''Public Service Company of Colorado Fort St. Vrain Nuclear Generating Station Updated Final Safety Analysis Report'', Docket No. 50-267, July 22, 1982 (Fig. 3.5-10).

7. SCOTT, C. B. and D. P. HARMON, ''Postirradiation Examination of Capsule F-30'', Document No. GA-A13208, April 1, 1975.

8. ''HTGR Fuel Technology Program Semiannual Report for the Period Ending September 30, 1982'', DOE Report GA-A16919, November 1982.

9. SAURWEIN, J. J., C. M. MILLER and C. A. YOUNG, ''Postirradiation Examination and Evaluation of Fort St. Vrain Fuel Element 1-0743, GA-A16258, May 1981.

10. HACKNEY, Rachel, ''Fort St. Vrain Cycle 2 Core Performance'', GAC-16743, April, 1982.

TITLE: METALLOGRAPHIC EXAMINATION OF A FUEL ROD FROM SEGMENT 2 FSV FUEL ELEMENT 1-2415

Document No. 906968 | Issue A

Table 1

COMPARISON OF BLOCKS WITH CRACKED WEBS

Item	S/N: 1-2415	S/N: 1-0172
Element Type	Fuel	Fuel
Core Location	08.05.F.06	08.05.F.07
Top Crack Width (mm) (Ref. 2)	0.20-0.25	0.13-0.15
Bottom Crack Width (mm) (ref. 2)	0.28-0.30	0.05-0.08
Temperature (^{o}C)[a]	650	700
Fluence (x 10^{25} n/m^2)[a]	1.55	1.28
Meas. Axial Strain (%)[b] $\pm$ 1σ	-0.337 $\pm$ 0.027	-0.163 + 0.010
Meas. Radial Strain (%)[b] $\pm$ 1σ	-0.257 $\pm$ 0.027	-0.089 $\pm$ 0.019
Meas. Bow (mm)	0.43	0.28
Gross γ Activity (R/h) at 91.5 cm[c]	458	385

(a) Temperature were obtained from SURVEY code calculations based on the GAUGE code depletion analysis of FSV Cycles 1 and 2. Fast neutron fluences were obtained from the GATT code depletion analysis of Cycles 1 and 2. Temperatures are for the graphite block time and volume averaged. The temperature uncertainty (1σ) is estimated at 10% of the difference between the block temperature and the (~335^{o}C, time averaged) gas-inlet temperature. The fast neutron fluences (E > 29 fJ)$_{HTGR}$ are volume averaged. The uncertainty in the fast fluence is $\pm$ 10% (1σ).

(b) Measured values came from the results of the metrology robot. (Ref. 1). Axial strains are element averages. Bow is at element midplane. Radial strains are element-averaged strains at the top of the blocks.

(c) Measured during nondestructive examination (see Ref. 1) with a Reuter-Stokes, Model RS-C4-1606-203, gamma ionization chamber.

Table 2

NOMINAL PREIRRADIATION FUEL ROD ATTRIBUTES FOR FSV SEGMENT 2 FUEL ELEMENT 1-2415

Fuel blend type: CR 16N-10167 Blend 1

Property	Acceptance Value
Preirradiation fission gas release, Kr-85m at 1100°C:	$\leq 3 \times 10^{-5}$
Heavy metal loadings	
U:	0.15 g/rod
Th:	4.13 g/rod
These requirements are for the average of all fuel rods in the core.	
Thorium contamination:	$\leq 8 \times 10^{-4}$
Impurities (ppm)	
B:	≤ 5
Fe:	≤ 500
S:	≤ 1200
Ti:	≤ 50
V:	≤ 50
Residual hydrogen:	≤ 200
Residual ash:	≤ 3000
H_2C:	*
Cl:	—
Firing temperature (°C):	1800

*--denostes no available data

TITLE: METALLOGRAPHIC EXAMINATION OF A FUEL ROD FROM SEGMENT 2 FSV FUEL ELEMENT 1-2415

Document No. 906968 | Issue A

Notations in this column indicate where changes have been made

Table 3

NOMINAL FISSILE FUEL PARTICLE ATTRIBUTES FOR
FSV FUEL ELEMENT S/N: 1-2415

Property	Acceptance Value
Kernel type:	$(Th,U)C_2$
Th/U mean ratio:	$3.60\ ^{+1.20}_{-0.20}$
Kernel A nominal diameter:	100 to 175 μm
Kernel B nominal diameter:	175 to 275 μm
Particle type:	TRISO
Mean Coating Parameters	
Mean thickness:	
Buffer:	25-75 μm
IPyC:	13-35 μm*
SiC:	15-35 μm
OPyC (Fissile A)	$\geq$20 μm
OPyC (Fissile B)	$\geq$25 μm
Mean density:	
Buffer:	0.75-1.40 Mg/m^3
IPyC:	1.70-2.00 Mg/m^3
SiC:	$\geq$3.16 Mg/m^3
OPyC:	1.60-2.00 Mg/m^3
Mean IPyC OPTAF:	$\leq$1.30
Mean OPyC OPTAF:	$\leq$1.25

*Combined thickness of seal plus inner-iso coatings.

TITLE: METALLOGRAPHIC EXAMINATION OF A FUEL ROD FROM SEGMENT 2 FSV FUEL ELEMENT 1-2415

Document No. 906908 | Issue A

Table 4

NOMINAL FERTILE FUEL PARTICLE ATTRIBUTES FOR FSV FUEL ELEMENT S/N: 1-2415

Property	Acceptance Value
Kernel type:	ThC_2
Particle type	TRISO
Kernel A nominal diameter:	300 to 410 μm
Kernel B nominal diameter:	410 to 500 μm
Mean Coating Parameters	
Mean thickness:	
Buffer:	35-75 μm
IPyC:	13-40*
SiC:	15-35 μm
OPyC (A)	$\geq$20 μm
OPyC (B)	$\geq$30 μm
Mean density:	
Buffer:	0.75-1.40 Mg/m^3
IPyC:	1.70-2.00 Mg/m^3
SiC:	$\geq$3.16 Mg/m^3
OPyC:	1.60-2.00 Mg/m^3
Mean IPyC OPTAF:	$\leq$1.30
Mean OPyC OPTAF:	$\leq$1.25

*Combined thickness of seal plus inner-iso coatings.

Notations in this column indicate where changes have been made

Table 5

FISSILE PARTICLE METALLOGRAPHIC EXAMINATION RESULTS

Property	Value
Time average fuel temperature (°C)	765[a]
Fast fluence x 10^{25} n/m^2 (E > 29 fJ)$_{HTGR}$	1.79[b]
Fissile FIMA (%)	8.35[c]
Number of particles examined	231
Buffer failure (%)[e]	3.0
IPyC failure (%)[e]	3.0
SiC failure (%)[e]	0.9
OPyC failure (%)[e]	0.4
Total coating failure (%)	N.D.[d]
Dispersion in buffer (%)	74.9
Dispersion in IPyC (%)	1.3
Debonding in IPyC (%)	42.9
SiC attack (%)	3.9
Flawed SiC coating (%)	0.4

(a) Taken from the SURVEY code, axial point 5, local points 4 and 5 (fuel temperature time-averaged).
(b) Data from Ref. (1).
(c) Data from Ref. 10.
(d) Not determined because the initial fuel rod mount hydrolyzed before any meaningful data could be gathered for the total coating failure.
(e) For each particle with coating failure, one or more intact coatings remained on the particle even though one coating was observed failed.

Table 6

FERTILE PARTICLE METALLOGRAPHIC EXAMINATION RESULTS

Property	Value
Time average fuel temperature (°C)	765[a]
Fast fluence x 10^{25} n/m^2 (E > 29 fJ)$_{HTGR}$	1.79[b]
Fertile FIMA (%)	0.61[c]
Number of particles examined	184
Buffer failure (%)[e]	18.5
IPyC failure (%)[e]	10.3
SiC failure (%)[e]	3.8
OPyC failure (%)[e]	7.6
Total coating failure (%)	N.D.[d]
Dispersion in buffer (%)	5.4
Dispersion in IPyC (%)	1.6
Debonding in IPyC (%)	12.0
SiC attack (%)	3.3
Flawed SiC coating (%)	6.5

(a) Taken from the SURVEY code, axial point 5, local points 4 and 5 (fuel temperature time-averaged).
(b) Data from Ref. (1).
(c) Data from Ref. 10.
(d) Not determined because the initial fuel rod mount hydrolyzed before any meaningful data could be gathered for the total coating failure.
(e) For each particle with coating failure, one or more intact coatings remained on the particle even though one coating was observed failed.

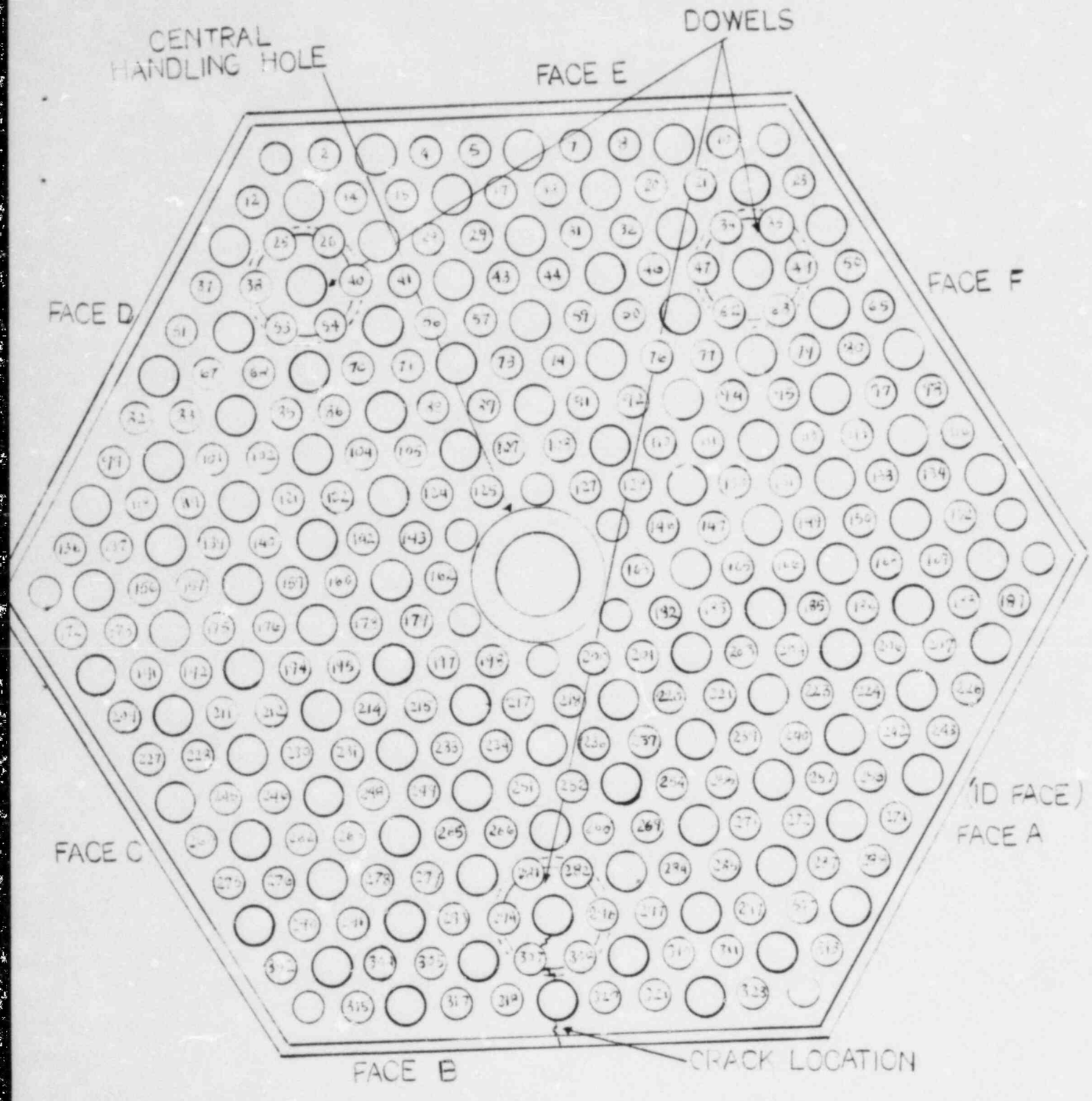

FIG. 1 FSV BLOCK FACE IDENTIFICATION

Notations in this column indicate where changes have been made

TITLE: METALLOGRAPHIC EXAMINATION OF A FUEL ROD FROM SEGMENT 2 FSV FUEL ELEMENT 1-2415

Document No. 906968 | Issue A

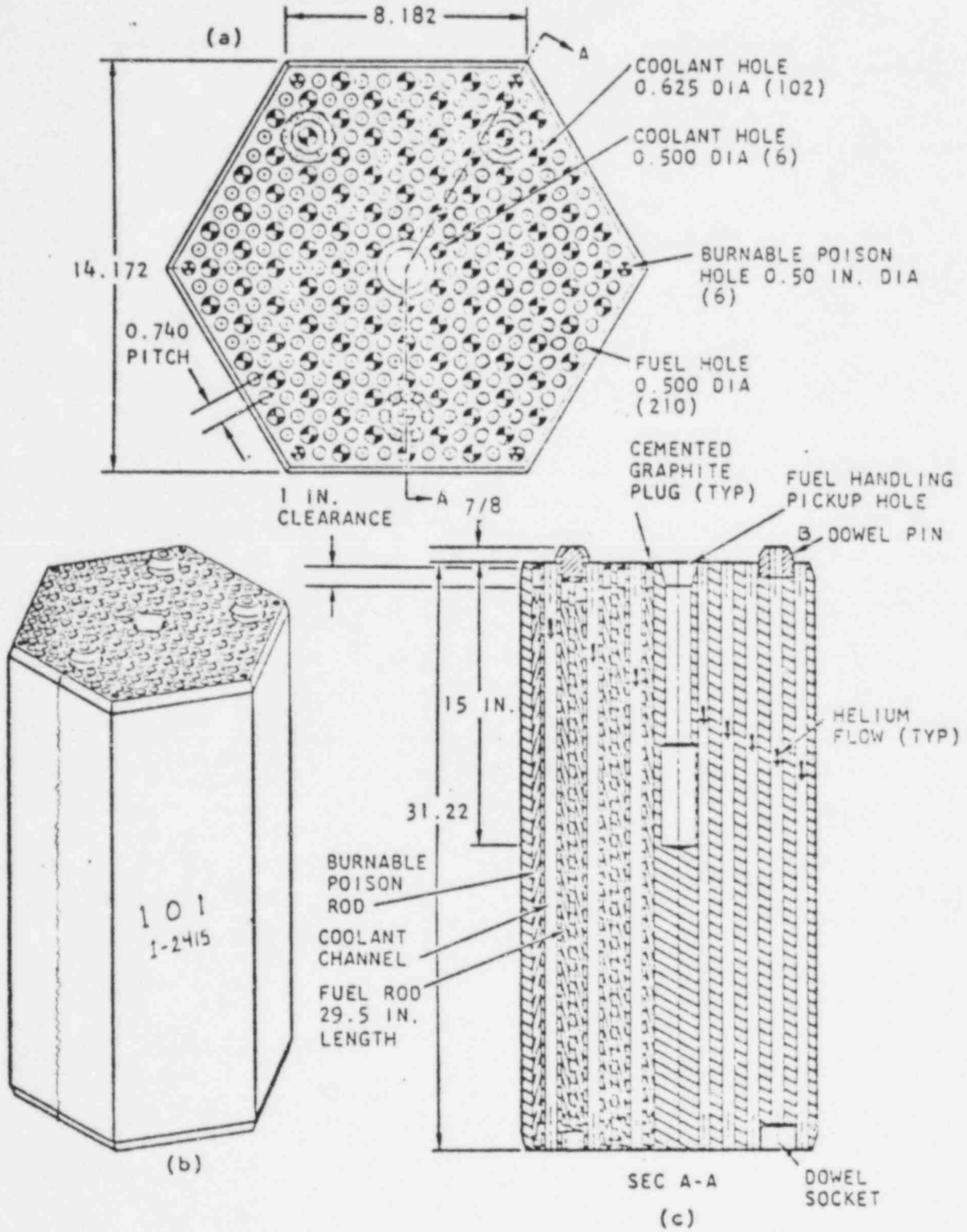

Fig. 2 Standard FSV fuel element 1-2415

Notations in this column indicate where changes have been made

TITLE: METALLOGRAPHIC EXAMINATION OF A FUEL ROD FROM SEGMENT 2 FSV FUEL ELEMENT 1-2415

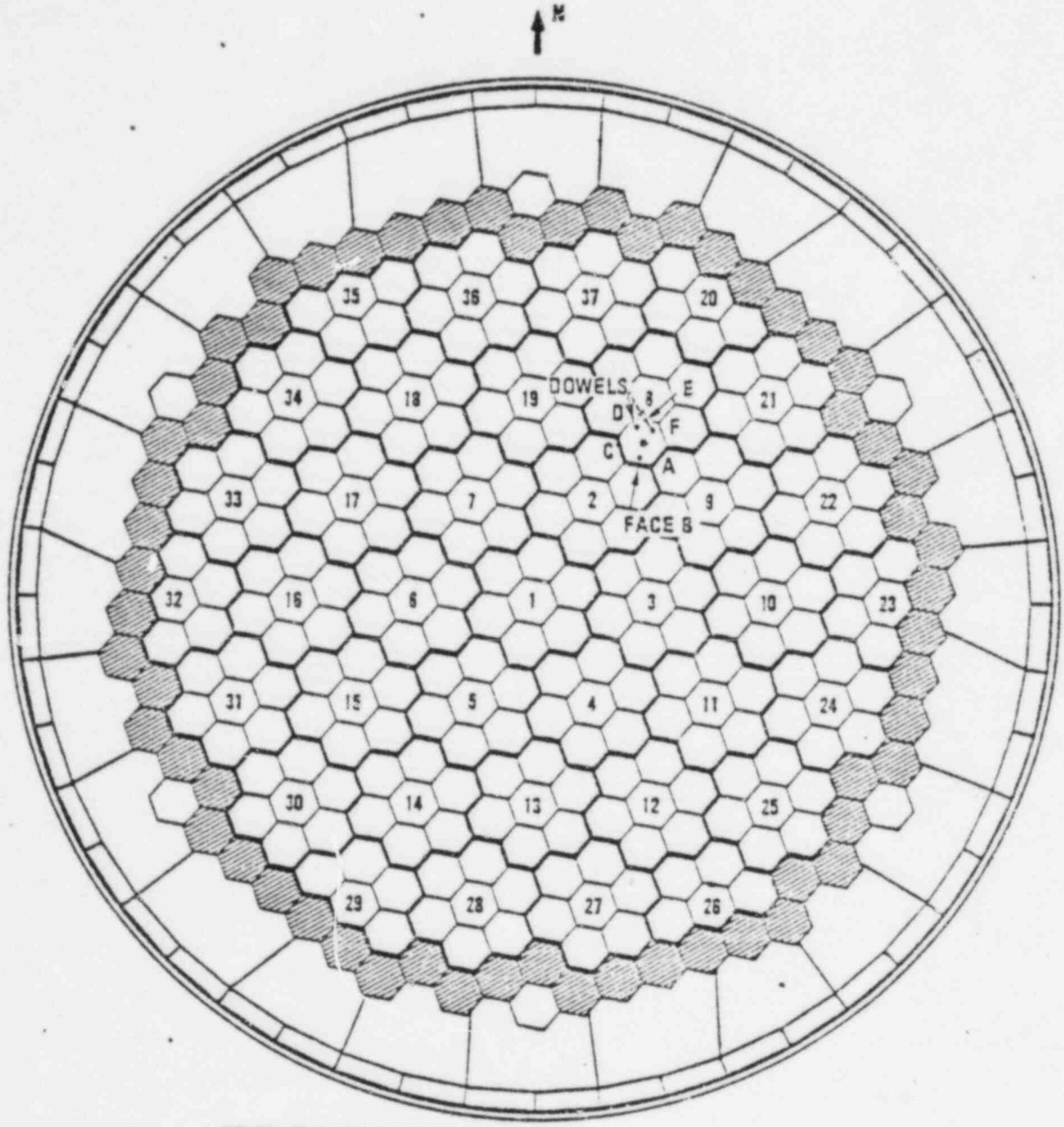

*FUEL ELEMENT 1-2415
REGION 8, COLUMN 5, CORE LAYER 6 (ACTIVE CORE LAYER 3)

Fig. 3 Core location of FSV fuel element 1-2415

TITLE: **METALLOGRAPHIC EXAMINATION OF A FUEL ROD FROM SEGMENT 2 FSV FUEL ELEMENT 1-2415**

Document No. 906968 | Issue A

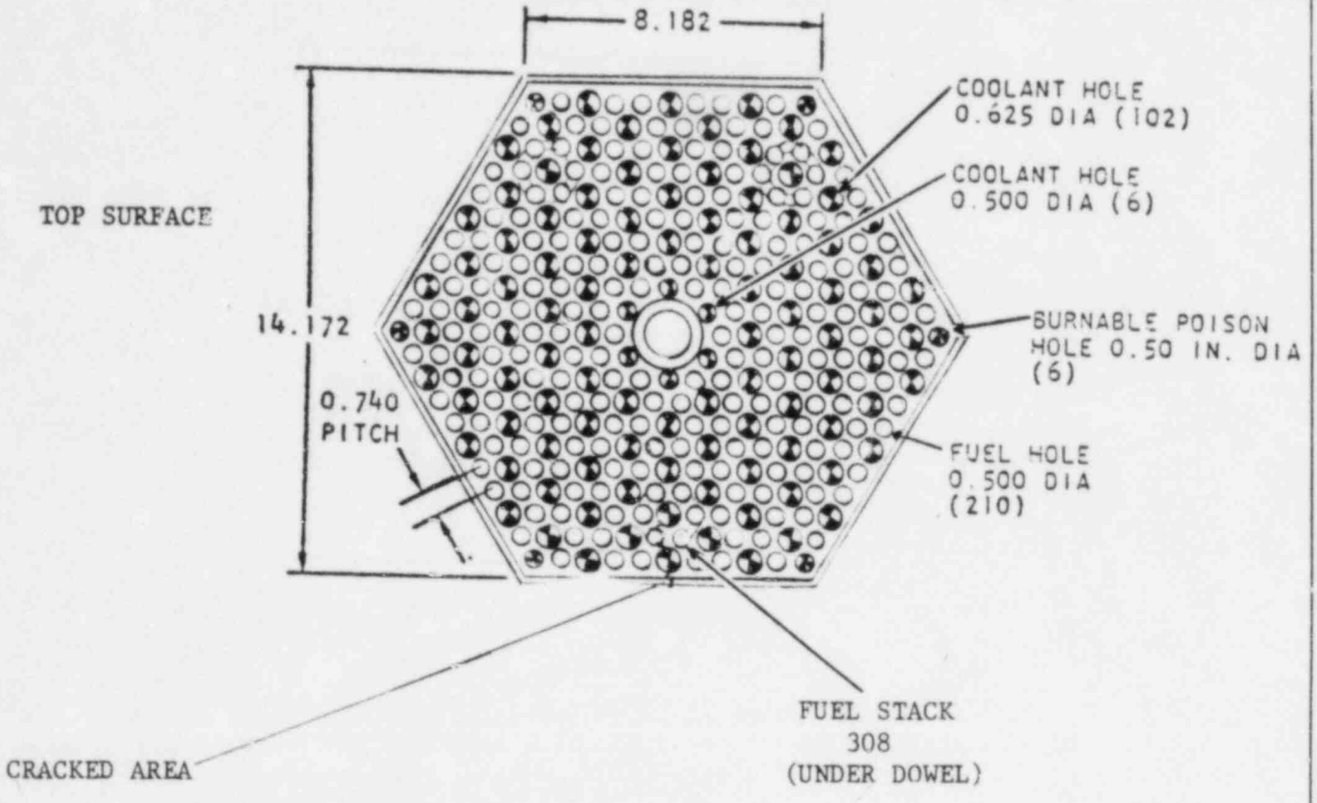

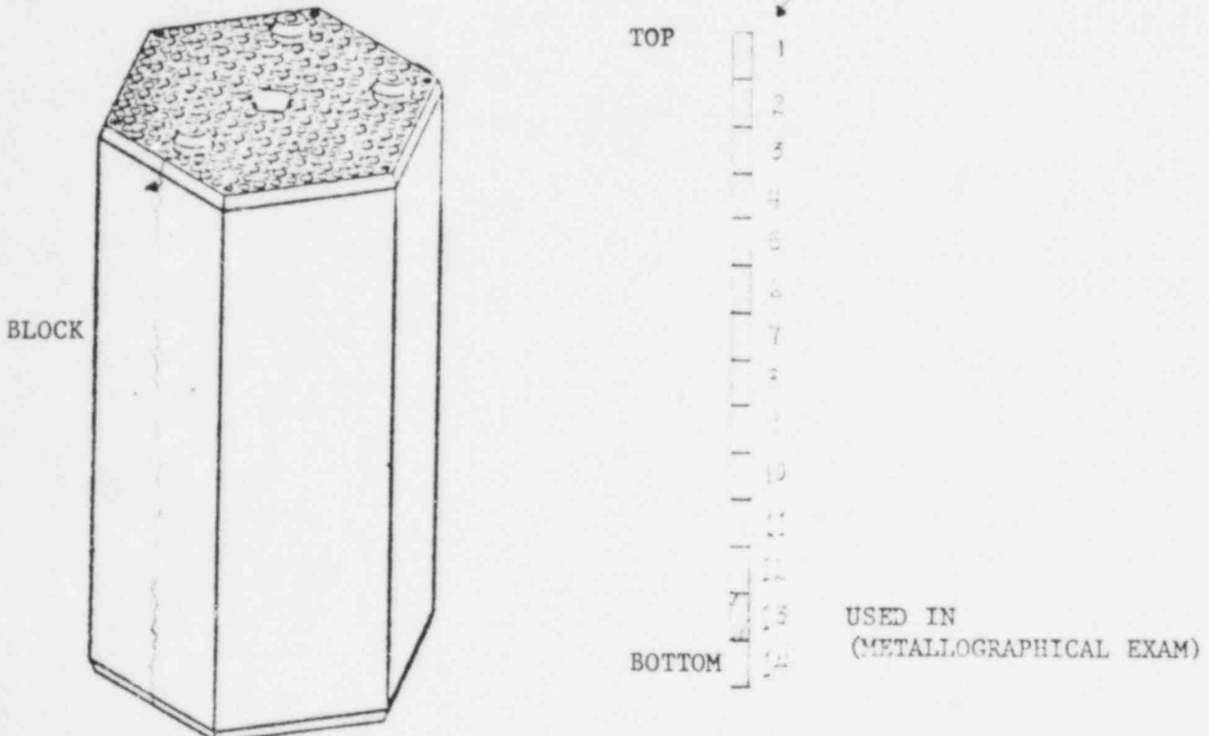

Fig. 4 Location of fuel rod used in metallography

TITLE: METALLOGRAPHIC EXAMINATION OF A FUEL ROD FROM SEGMENT 2 FSV FUEL ELEMENT 1-2415

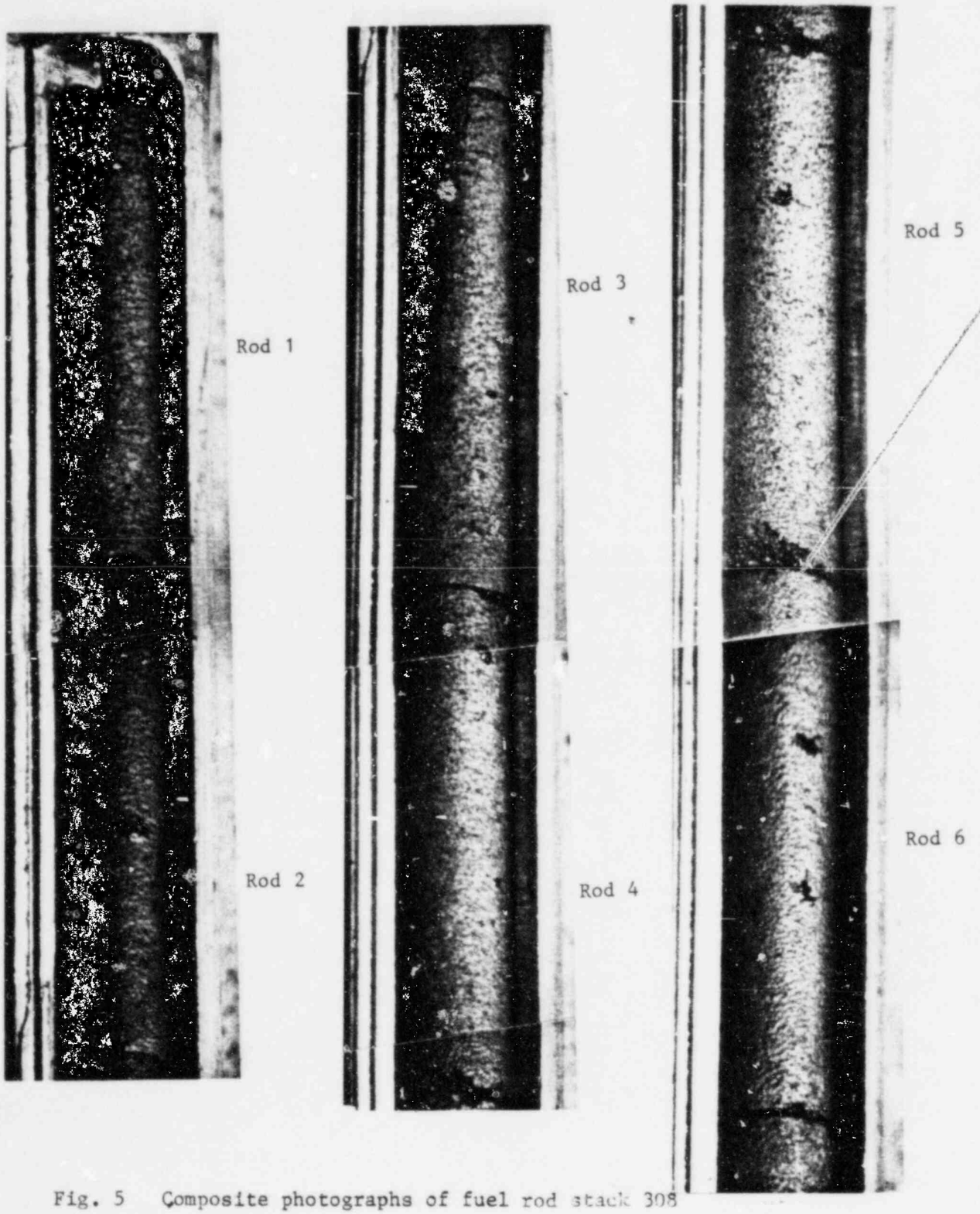

Fig. 5 Composite photographs of fuel rod stack 308

GA-1484 (REV. 10/82)

TITLE: **METALLOGRAPHIC EXAMINATION OF A FUEL ROD FROM SEGMENT 2 FSV FUEL ELEMENT 1-2415**

Document No. 906968 | Issue A

Notations in this column indicate where changes have been made

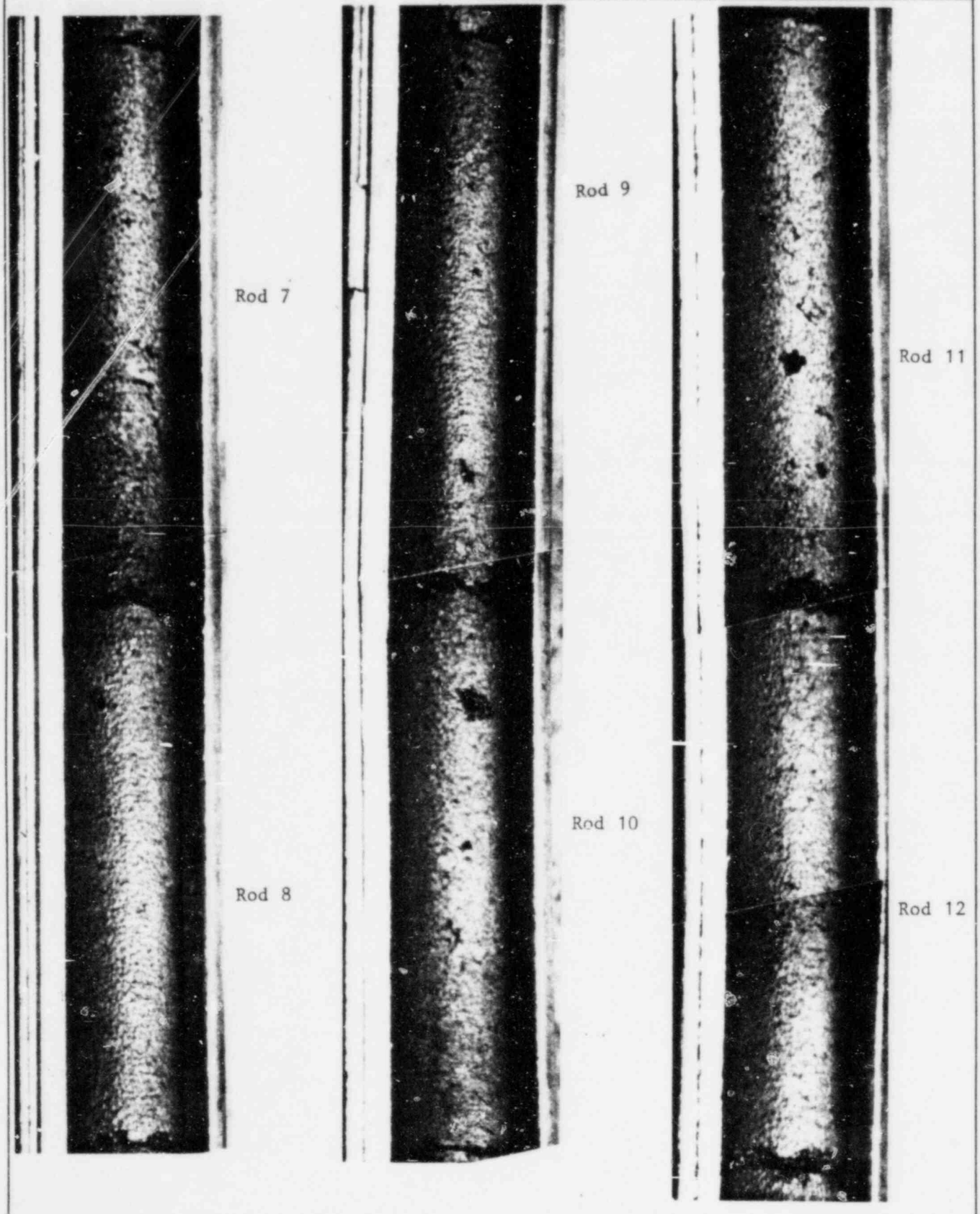

Fig. 5 Composite photographs of fuel rod stack 308 (con't)

TITLE: METALLOGRAPHIC EXAMINATION OF A FUEL ROD FROM SEGMENT 2 FSV FUEL ELEMENT 1-2415

Rod 13

Rod 14

Fig. 5 Composite photographs of fuel rod stack 308 (con't)

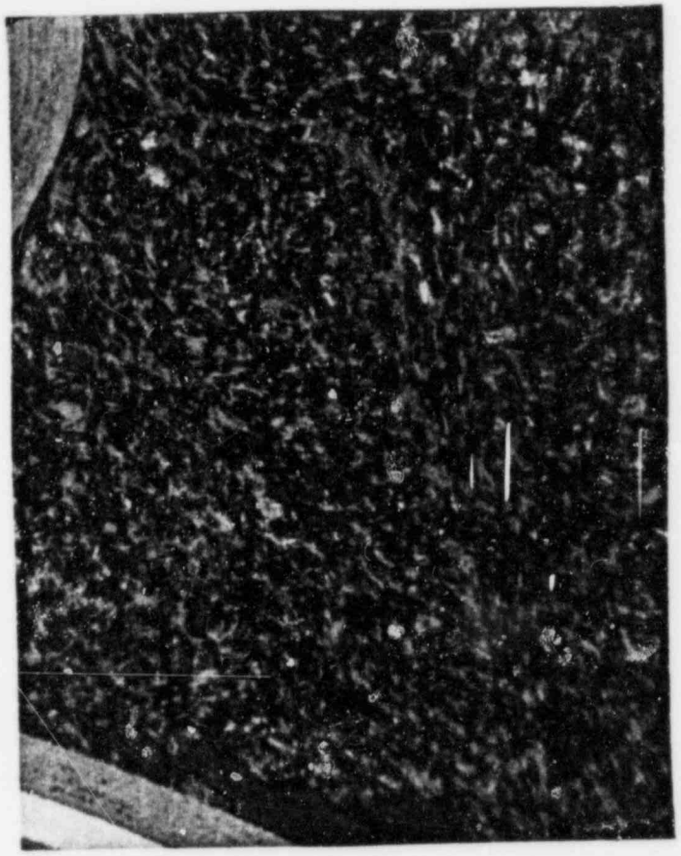

8320-30

33 µm

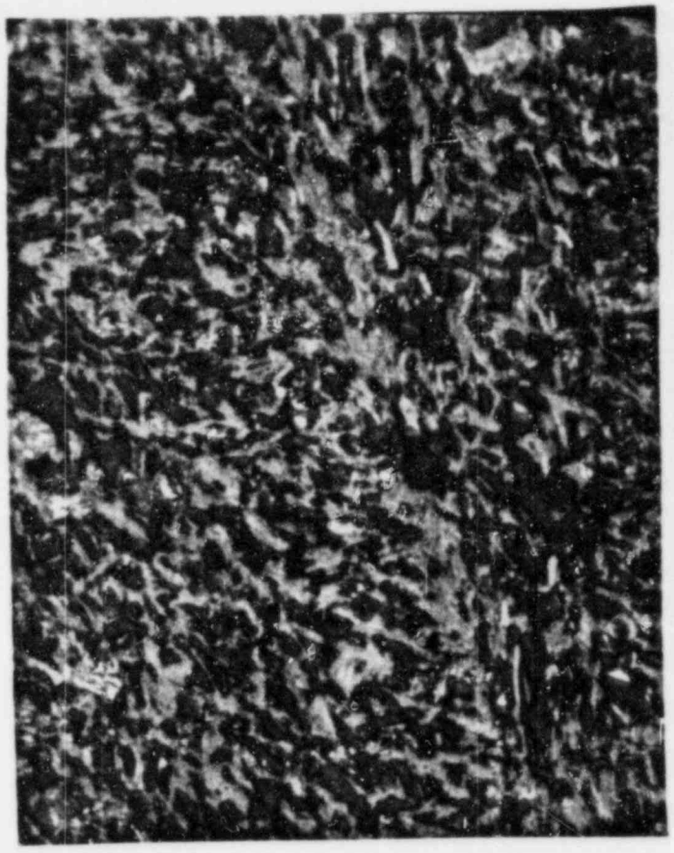

8320-31

15 µm

Fig. 6 Photomicrographs representative of matrix phase of irradiated rod 13 from stack 308. The time average fuel temperature was approximately 765°C at an average fast fluence of 1.6×10^{25} n/m^2 (E > 29 fJ)$_{HTGR}$

TITLE: METALLOGRAPHIC EXAMINATION OF A FUEL ROD FROM SEGMENT 2 FSV FUEL ELEMENT 1-2415

Document No. 906968 | Issue A

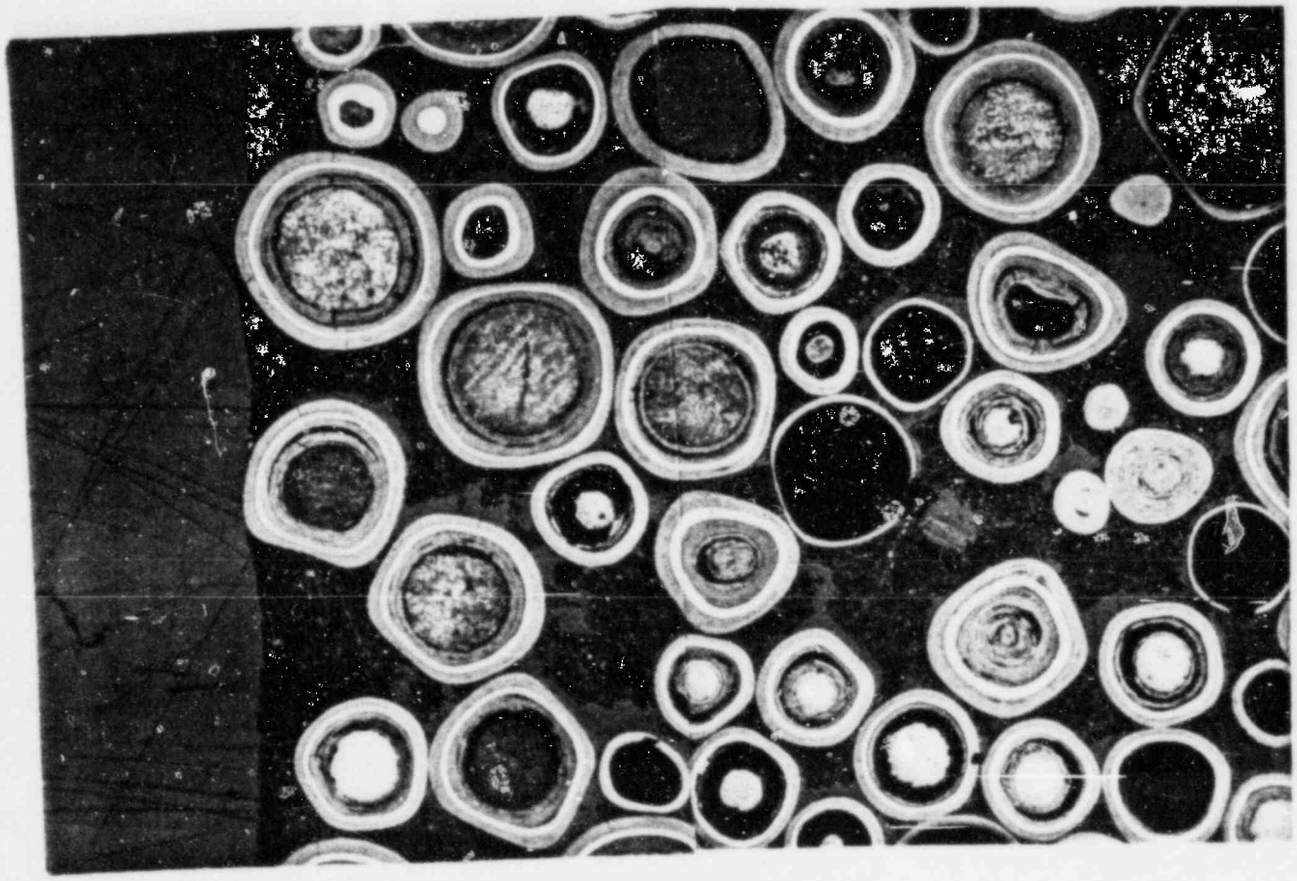

Fig. 7 Representative photomicrographs of composite of radial cross section of fuel rod from FSV element 1-2415 (left side of rod)

TITLE: METALLOGRAPHIC EXAMINATION OF A FUEL ROD FROM SEGMENT 2 FSV FUEL ELEMENT 1-2413

Document No. 906968 | Issue A

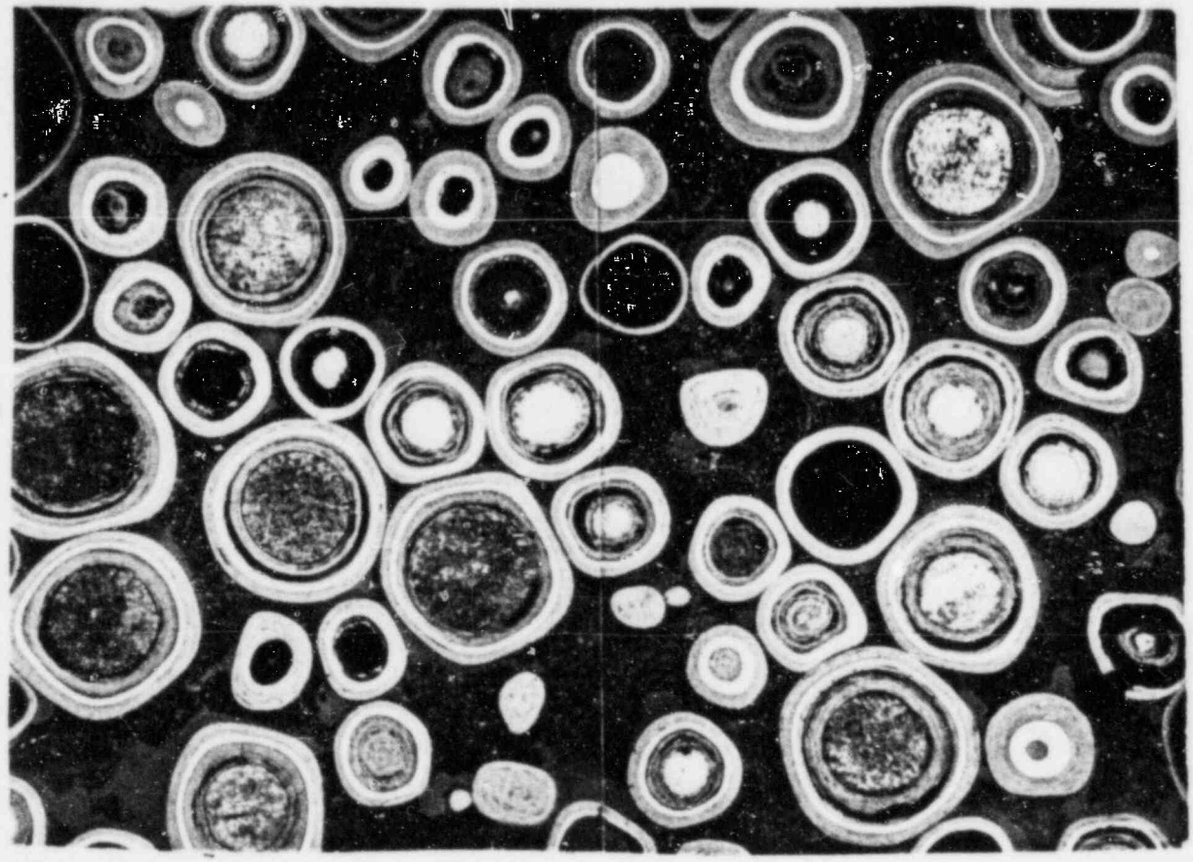

Fig. 7 (con't) Representative photomicrographs of composite of radial cross section of fuel rod from FSV element 1-2415 (middle of rod)

TITLE: METALLOGRAPHIC EXAMINATION OF A FUEL ROD FROM SEGMENT 2 FSV FUEL ELEMENT 1-2415

Document No. 906968 | Issue A

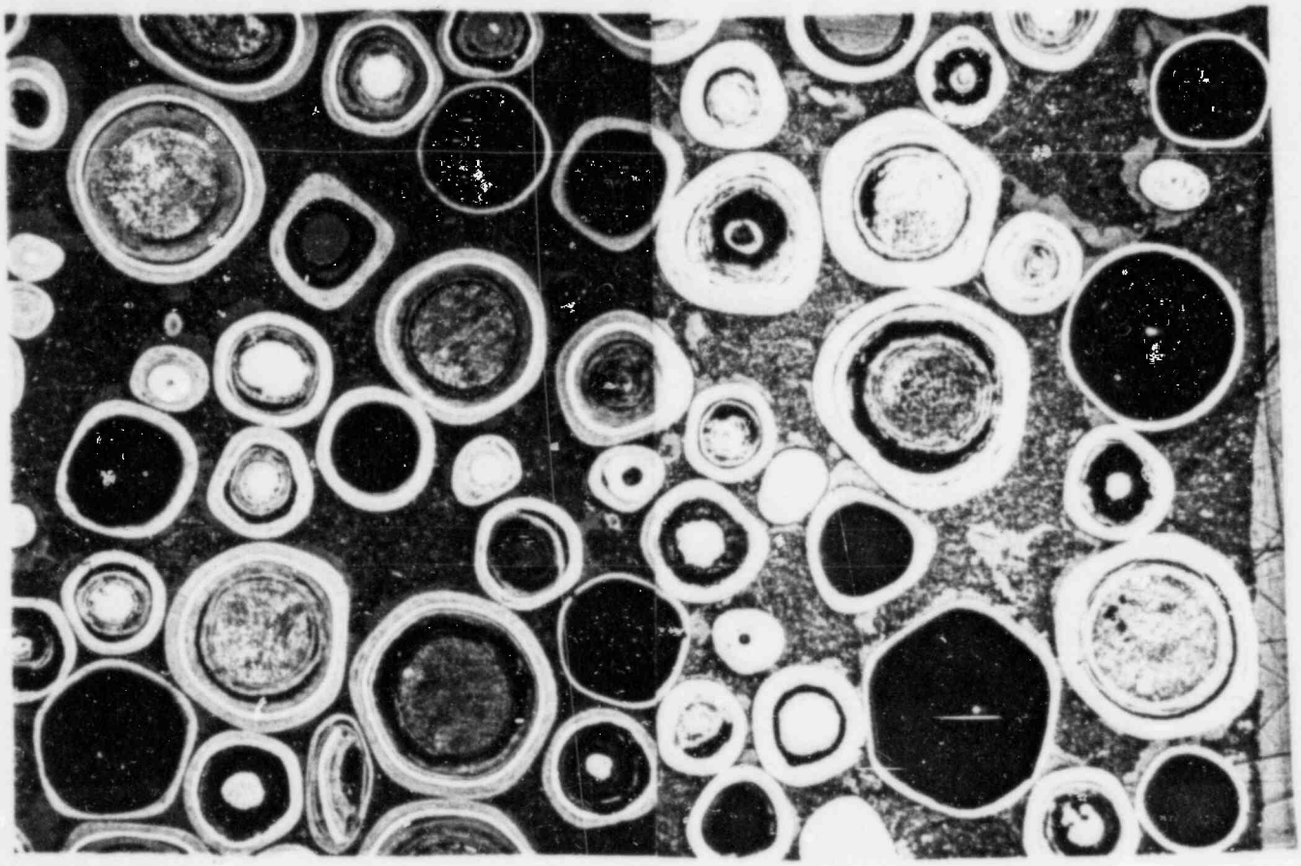

Fig. 7 (con't) Representative photomicrographs of composite of radial cross section of fuel rod from FSV element 1-2415 (right side of rod)

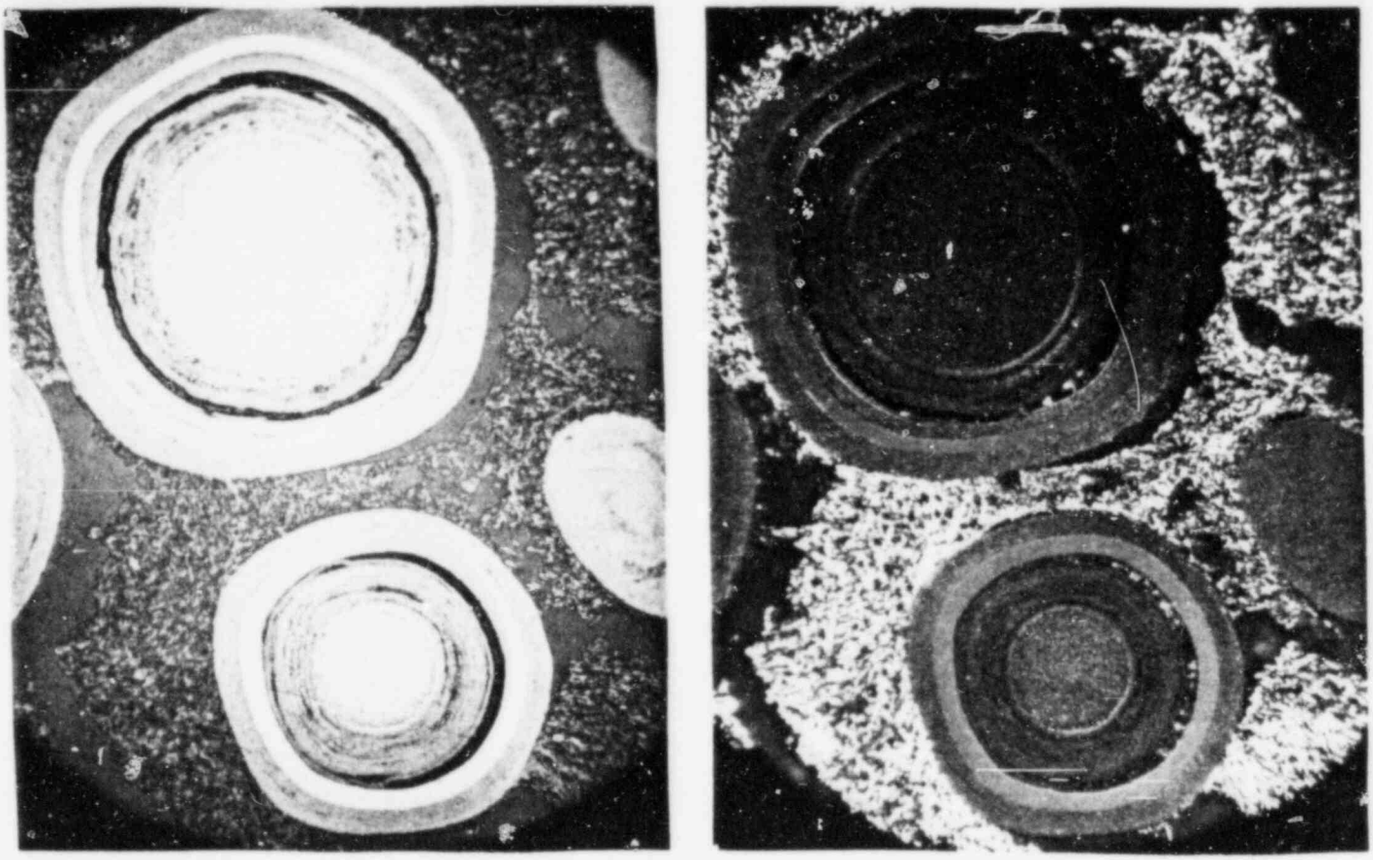

Fig. 8 Photomicrographs of fissile (a,b) and fertile (c) particles. (a) and (c) are bright field illuminated and (b) is polarized light.

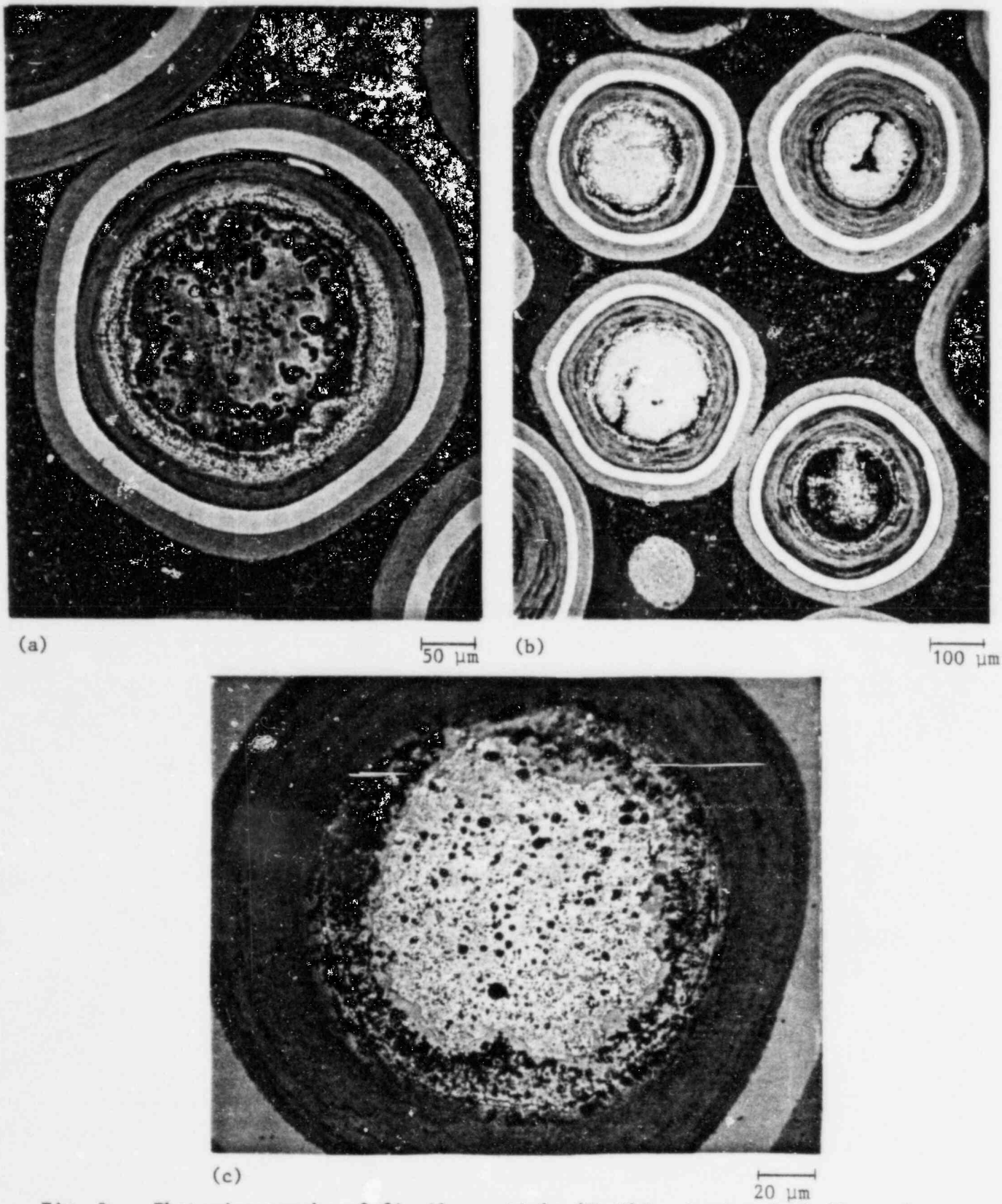

Fig. 9 Photomicrographs of fissile particle $(Th,U)C_2$ showing fuel dispersion. Note the dense phase in the buffer coatings and the low-density IPyC coating.

TITLE: **METALLOGRAPHIC EXAMINATION OF A FUEL ROD FROM SEGMENT 2 FSV FUEL ELEMENT 1-2415**

Document No. **906968** | Issue **A**

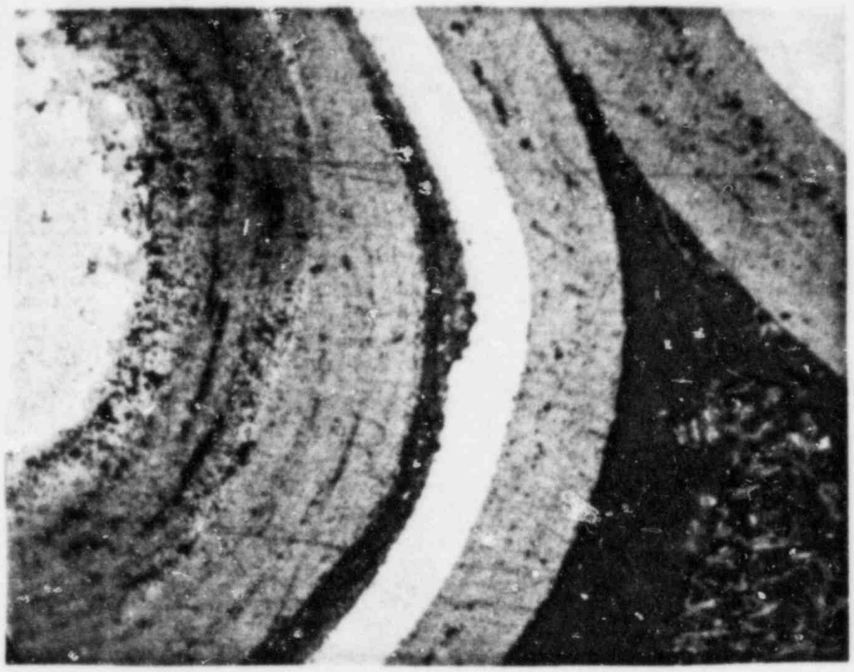

(a) 20 μm

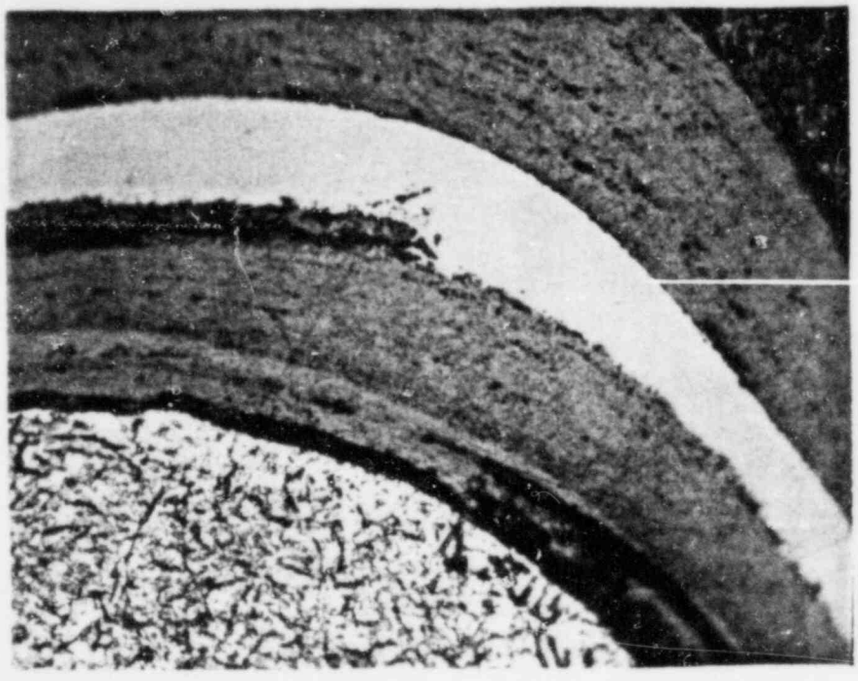

(b) 20 μm

Fig. 10 Photomicrographs showing SiC-fission product interaction in the fissile (a) and fertile (b) particles

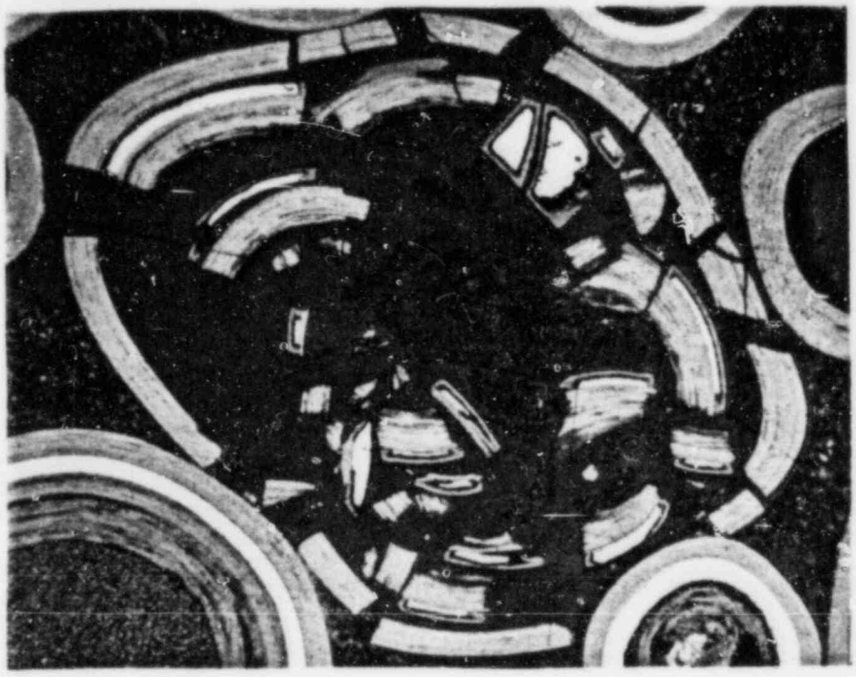

Fig. 11 Photomicrograph of an as-manufactured defective particle in an irradiated fuel rod. Note total coating failure with the matrix pressed in the particle. Also, note that the kernel has been leached out.

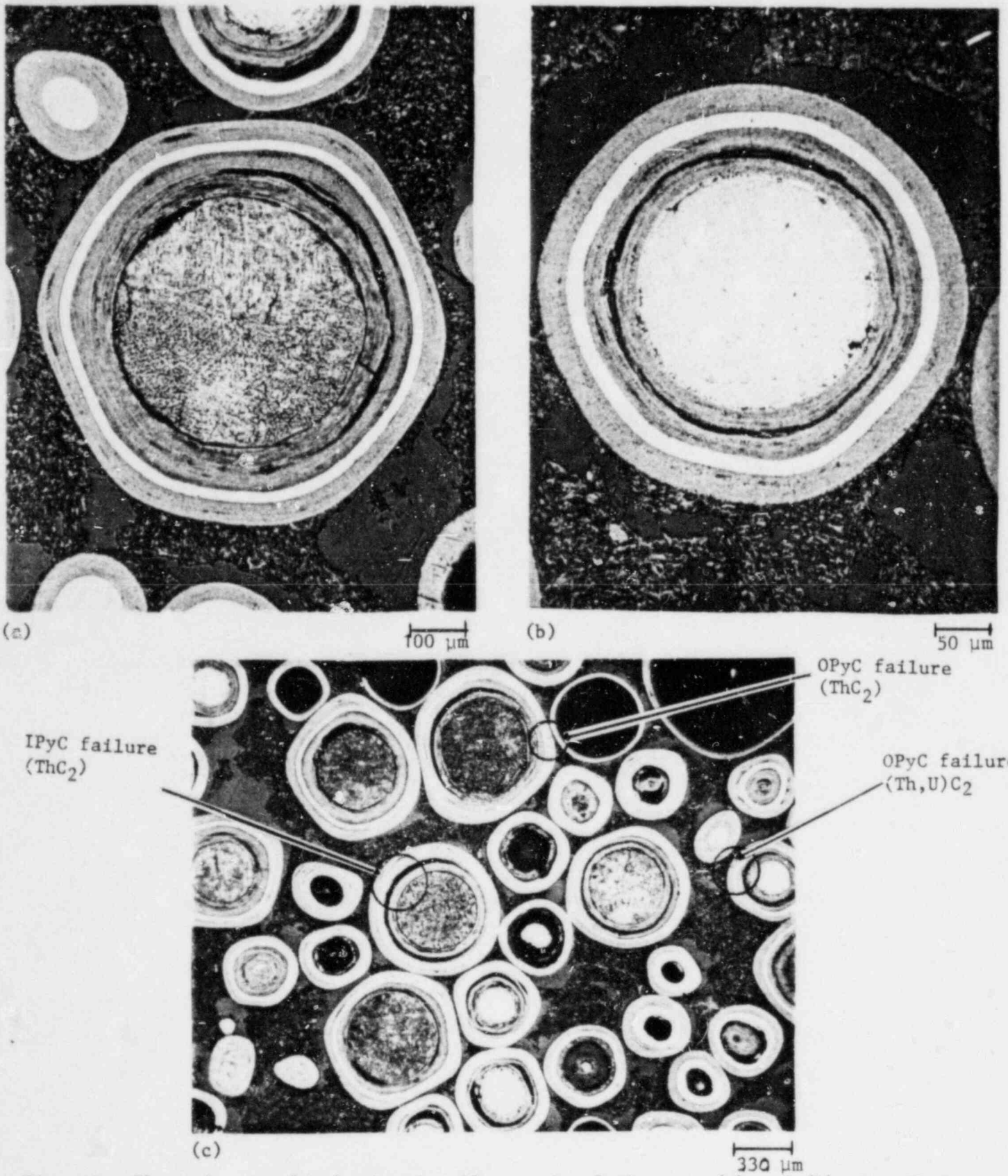

Fig. 12 Photomicrographs showing in-pile coating failures. (a) and (b) show IPyC failures in the fertile and fissile particles, respectively. (c) Shows examples of OPyC and IPyC failures in the fertile particle and OPyC failure in the fissile particle.